9-25-2017

γ -rigid solution of the Bohr Hamiltonian for the critical point description of the spherical to γ -rigidly deformed shape phase transition

Yu Zhang
Liaoning Normal University

Feng Pan
Liaoning Normal University

Yu Xin Liu
Peking University

Yan An Luo
Nankai University

J. P. Draayer
Louisiana State University

Recommended Citation
Zhang, Y., Pan, F., Liu, Y., Luo, Y., & Draayer, J. (2017). γ -rigid solution of the Bohr Hamiltonian for the critical point description of the spherical to γ -rigidly deformed shape phase transition. *Physical Review C, 96* (3) https://doi.org/10.1103/PhysRevC.96.034323

γ-rigid solution of the Bohr Hamiltonian for the critical point description of the spherical to γ-rigidly deformed shape phase transition

Yu Zhang, Feng Pan, Yu-Xin Liu, Yan-An Luo, and J. P. Draayer

Phys. Rev. C **96**, 034323 — Published 25 September 2017

DOI: 10.1103/PhysRevC.96.034323

γ-rigid solution of the Bohr Hamiltonian for the critical point description of the spherical to γ-rigidly deformed shape phase transition

Yu Zhang,[1] Feng Pan,[1,2] Yu-Xin Liu,[3,4,5] Yan-An Luo,[6] and J. P. Draayer[2]

[1]*Department of Physics, Liaoning Normal University, Dalian 116029, P. R. China*
[2]*Department of Physics and Astronomy, Louisiana State University, Baton Rouge, LA 70803-4001, USA*
[3]*Department of Physics and State Key Laboratory of Nuclear Physics and Technology, Peking University, Beijing 100871, P. R. China*
[4]*Collaborative Innovation Center of Quantum Matter, Beijing 100871, China*
[5]*Center for High Energy Physics, Peking University, Beijing 100871, China*
[6]*School of Physics, Nankai University, Tianjin 300071, P. R. China*

(Dated: August 20, 2017)

γ-rigid solution of the Bohr Hamiltonian with the β-soft potential and $0^\circ \leq \gamma \leq 30^\circ$ is worked out. The resulting model, called T(4), provides a natural dynamical connection between the X(4) and the Z(4) critical point symmetries, which thus serves as the critical point symmetry of the spherical to γ-rigidly deformed shape phase transition. This point is further justified through comparing the model dynamics with those of the interacting boson model. As a preliminary test, the low-lying structures of ^{158}Er are taken to compare the theoretical calculations, and the results indicate that this nucleus could be considered as the candidate of the T(4) model with an intermediate γ-deformation.

PACS numbers: 21.60.Ev, 21.60.Fw, 21.10.Re

1. Introduction

Critical point symmetries (CPSs) in nuclear structure have attracted a lot of attentions [1–13] since the CPSs provide the parameter-free (up to an overall scale) predictions about the structural properties of nuclei in the transitional region [14, 15]. The typical CPSs include, for example, the CPS of the spherical to γ-unstable shape phase transition E(5) [1], the CPS of the spherical to axially deformed shape phase transition X(5) [2], the CPS of the axial to triaxial shape phase transition Y(5) [3], and the CPS of the prolate to oblate shape phase transition Z(5) [4], etc, which have been widely confirmed in experiment [15]. Generally, these CPSs come exactly or approximately [16] from the Bohr Hamiltonian [17] with suitable β- and γ-potentials based on the physical situations studied.

Most recently, a new four-dimensional CPS model [13], called X(4), has been introduced [13, 18, 19]. It was suggested that the X(4) model can be applied to describe the critical point of the U(5)-SU(3) shape phase transition (or the spherical to axially-deformed shape phase transition) in the interacting boson model (IBM) [20]. Another four-dimensional CPS model [5], called Z(4), which is obtained from the Bohr Hamiltonian with γ frozen at $\gamma = 30^\circ$, is shown to have spectral properties similar to those of the E(5) CPS [1] since γ-unstable models and γ-rigid models may yield similar predictions for most observables if the averaged value of γ of the former, $\gamma_{\rm av}$, is equal to $\gamma_{\rm rigid}$ of the latter [21, 22]. It means that the Z(4) model can also serve as the CPS of the U(5)-O(6) shape phase transition (or the spherical to γ-unstable shape phase transition) in the IBM [20]. The X(4) and Z(4) CPSs [5, 13] have some common features: Both models employ the infinite square well potential to simulate the β-soft situation in the transitional region; and the effective model space of the two models is both four dimensional. It is imperative to explore the dynamical symmetry in between the X(4) and the Z(4), which may provide a hallmark for the critical points of more general transitions from spherical to γ-rigidly deformed or to the γ-unstable shape.

In this work, a Bohr Hamiltonian with the suitable β-soft potential and for a fixed value of γ with $0^\circ \leq \gamma \leq 30^\circ$ as used in Ref. [23] will be studied, which is called T(4) in accordance to the previous terminology. It will be shown that the T(4) model provides a natural dynamical connection between the X(4) and the Z(4) CPSs [5, 13], and thus serves as the CPS for the more general spherical to γ-rigidly deformed or to the γ-unstable shape phase transitions.

2. The model

In the model of Davydov and Chaban [23], the Bohr Hamiltonian with a γ-rigid deformation is written as

$$H = -\frac{\hbar^2}{2B}\Big[\frac{1}{\beta^3}\frac{\partial}{\partial\beta}\beta^3\frac{\partial}{\partial\beta} - \frac{1}{4\beta^2}\sum_k \frac{L_k'^2}{\sin^2(\gamma-\frac{2}{3}k\pi)}\Big] + U(\beta), \quad (1)$$

where β and γ are the usual collective coordinates, B is the collective mass parameter, and L'_k ($k = 1,\ 2,\ 3$) are the projections of the angular momentum on the body-fixed k-axis. In this case, the variable γ is treated as a parameter of the axial asymmetry of a nucleus. Hence, the Hamiltonian only depends on four variables (β, θ_i), which means that only β vibrations of the nuclear surface and rotation of the nucleus are considered [23]. Although the Hamiltonian (1) was originally introduced to describe triaxially deformed nuclei [23] corresponding to $\gamma > 0$, the axial-symmetry limit ($\gamma = 0$) is also well-defined, which indicates that the parameter $\gamma \in [0,\ 30^\circ]$ is physically allowed for the Hamiltonian (1).

In both the vibration to axially deformed and to γ-unstable shape phase transition regions, the deformation of nucleus is more or less β-soft. Here β-softness means that the β-deformation of nucleus is soft within a confined range of

β values thus connected with a flat potential bottom rather than a fully β-independent structure, which is actually consistent with the "confined β-soft" (CBS) situation proposed by Pietralla and Gorbachenko in [11]. To describe this feature, the β-potential is usually assumed as [1, 2, 11]

$$U(\beta)=\begin{cases}0, & \beta\le\beta_W,\\ \infty, & \beta>\beta_W.\end{cases} \tag{2}$$

By introducing reduced energy $\varepsilon=2BE/\hbar^2$ and reduced potential $u=2BU/\hbar^2$ [2, 4], the separation of variables for the differential equation $H\Psi(\beta,\theta_i)=E\Psi(\beta,\theta_i)$ with $\Psi(\beta,\theta_i)=\eta_L(\beta)\varphi^L_{M,s}(\theta_i)$, where θ_i ($i=1,\ 2,\ 3$) are the Euler angles, leads to two equations:

$$\Big[-\frac{1}{\beta^3}\frac{\partial}{\partial\beta}\beta^3\frac{\partial}{\partial\beta}+\frac{r_L}{4\beta^2}+u(\beta)\Big]\eta_L(\beta)=\varepsilon_\beta\eta_L(\beta) \tag{3}$$

and

$$\sum_k\frac{L'^2_k}{\sin^2(\gamma-\frac{2}{3}k\pi)}\varphi^L_{M,s}(\theta_i)=r_{L_s}\varphi^L_{M,s}(\theta_i), \tag{4}$$

where r_L is the eigenvalue of the rotational energy.

The rotational wave function $\varphi^L_{M,s}(\theta)$ can further be expressed as [12]

$$\varphi^L_{M,s}(\theta_i)=\sum_K C^L_{s,K}\chi^L_{M,K}(\theta_i) \tag{5}$$

with

$$\chi^L_{M,K}(\theta_i)=\sqrt{\frac{2L+1}{16\pi^2(1+\delta_{K,0})}}\times[D^L_{M,K}(\theta_i)+(-1)^LD^L_{M,-K}(\theta_i)], \tag{6}$$

where $D^L_{M,K}(\theta_i)$ is the Wigner D-function. The expansion coefficients $C^L_{s,K}$ are determined by Eq. (4), and s is used to label the s-th eigenstate for given L and M with [12]

$$s=1,\ 2,\ 3,\ 4,...,\ \frac{2L+3(-1)^L+1}{4}. \tag{7}$$

In case of $\gamma=0^\circ$, the value of r_L is analytically given as

$$r_L(0^\circ)=\frac{4}{3}L(L+1). \tag{8}$$

The resulting model just corresponds to the X(4) CPS [13]. The present result shows that the X(4) CPS can be alternatively explained as the $\gamma\to0^\circ$ solution of the model. The exact axial-symmetry in case of $\gamma=0^\circ$ requires that arbitrary rotation around the symmetric axis of the system is quantum mechanically undetectable [24, 25], which indicates that only the $K=0$ bands are allowed in this case. It should be mentioned that a more rigorous derivation of the Bohr Hamiltonian with γ frozen at $\gamma=0^\circ$ before its quantization leads to the X(3) Hamiltonian [6] rather than the X(4) Hamiltonian [13], since the γ-rigid condition $\dot\gamma=0$ and the axial-symmetry condition $\gamma=0^\circ$ imposed on the classical form of the Bohr Hamiltonian may reduce the system directly to that with three degrees of freedom [6]. For $\gamma=30^\circ$, one can derive

$$r_L(30^\circ)=4L(L+1)-3\alpha^2 \tag{9}$$

with α being the projection of the angular momentum on the body-fixed 1-axis. In this case, the resulting model corresponds to the Z(4) CPS [5]. The above discussions indicate that the original X(4) and Z(4) CPSs are the two limit situations of the model. It is undoubtable that the solutions of the Hamiltonian (1) with β-potential expressed in Eq. (2) and $\gamma\in[0^\circ,30^\circ]$ provide a dynamical connection between the X(4) and the Z(4) CPSs. We refer thus this model as the T(4) model.

For cases with $0^\circ<\gamma<30^\circ$, the values of r_L can only be numerically but exactly solved from Eq. (4). Particularly, r_{L_s} with $s\le2$ for some low L values can be expressed analytically [26, 27], *viz.*

$$r_{0_{s=1}}(\gamma)=0, \tag{10}$$

$$r_{2_{s=1}}(\gamma)=\frac{18-6\sqrt{9-8\sin^2(3\gamma)}}{\sin^2(3\gamma)}, \tag{11}$$

$$r_{2_{s=2}}(\gamma)=\frac{18+6\sqrt{9-8\sin^2(3\gamma)}}{\sin^2(3\gamma)}, \tag{12}$$

$$r_{3_{s=1}}(\gamma)=\frac{36}{\sin^2(3\gamma)}, \tag{13}$$

$$r_{5_{s=1}}(\gamma)=\frac{90-18\sqrt{9-8\sin^2(3\gamma)}}{\sin^2(3\gamma)}, \tag{14}$$

$$r_{5_{s=2}}(\gamma)=\frac{90+18\sqrt{9-8\sin^2(3\gamma)}}{\sin^2(3\gamma)}. \tag{15}$$

The corresponding expansion coefficients $C^L_{s,K}$ defined in Eq. (5) can be analytically written as

$$C^0_{1,0}(\gamma)=1, \tag{16}$$

$$C^2_{1,0}(\gamma)=\cos(\Gamma),\ \ C^2_{1,2}(\gamma)=-\sin(\Gamma), \tag{17}$$

$$C^2_{2,0}(\gamma)=\sin(\Gamma),\ \ C^2_{2,2}(\gamma)=\cos(\Gamma), \tag{18}$$

$$C^3_{1,2}(\gamma)=1, \tag{19}$$

$$C^5_{1,2}(\gamma)=\cos(\Gamma),\ \ C^5_{1,4}(\gamma)=-\sin(\Gamma), \tag{20}$$

$$C^5_{2,2}(\gamma)=\sin(\Gamma),\ \ C^5_{2,4}(\gamma)=\cos(\Gamma), \tag{21}$$

where [27]

$$\Gamma=-\frac{1}{2}\arccos\Big[\frac{\cos(4\gamma)+2\cos(2\gamma)}{\sqrt{9-8\sin^2(3\gamma)}}\Big]. \tag{22}$$

Substituting $F(\beta)=\beta\eta(\beta)$ and $z=\beta k_\beta$ with $k_\beta=\sqrt{\varepsilon_\beta}$, one can transform Eq. (3) inside the well into the Bessel equation

$$\frac{d^2F}{dz^2}+\frac{1}{z}\frac{dF}{dz}+\Big[1-\frac{v^2}{z^2}\Big]F=0 \tag{23}$$

with

$$v = \sqrt{\frac{r_L}{4}+1}\,. \tag{24}$$

The boundary condition $\eta(\beta_W)=0$ determines the eigenvalues

$$\varepsilon_{\beta;\xi,s,L} = (k_{\xi,v})^2, \quad k_{\xi,v} = \left(\frac{x_{\xi,v}}{\beta_W}\right), \tag{25}$$

and the eigenfunction

$$\eta_{\xi,s,L}(\beta) = c_{\xi,v}\beta^{-1}J_v(k_{\xi,v}\beta)\,, \tag{26}$$

where $x_{\xi,v}$ is the ξ-th zero of the Bessel function $J_v(z)$, and the normalization constants $c_{\xi,v}$ are determined by

$$\int_0^{\beta_w}\beta^3\eta^2_{\xi,s,L}(\beta)d\beta = 1\,. \tag{27}$$

$B(E2)$ values can be calculated by taking the quadrupole operator

$$\begin{aligned} T^{E2}_u &= t\beta[D^{(2)}_{u,0}(\theta_i)\cos(\gamma) \\ &\quad + \frac{1}{\sqrt{2}}(D^{(2)}_{u,2}(\theta_i)+D^{(2)}_{u,-2}(\theta_i))\sin(\gamma)]\,, \end{aligned} \tag{28}$$

where t is a scale factor. Specifically, we have

$$B(E2;L_i\xi_i s_i\rightarrow L_{f\,\xi_f s_f}) = \frac{|\,\langle\xi_f L_f s_f\parallel T^{E2}\parallel\xi_i L_i s_i\rangle\,|^2}{2L_i+1}\,. \tag{29}$$

In the calculation, the integral over β takes the form

$$\begin{aligned} &I_\beta(\xi_i,\,s_i,\,L_i;\,\xi_f,\,s_f,\,L_f) \\ &\quad = \int_0^{\beta_w}\beta\,\eta_{\xi_i,s_i,Li}(\beta)\eta_{\xi_f,s_f,Lf}(\beta)\beta^3 d\beta\,, \end{aligned} \tag{30}$$

while the integral over the Euler angles θ_i can be obtained by making use of the formula involving three Wigner D-functions [28]. The final result is given as

$$\begin{aligned} &B(E2;L_i\xi_i s_i\rightarrow L_{f\,\xi_f s_f}) \\ &= t^2 I^2_\beta(\xi_i,s_i,L_i;\xi_f,s_f,L_f) \\ &\quad\times\Big\{\sum_{K_i,K_f}\sqrt{\frac{1}{(1+\delta_{K_i0})(1+\delta_{K_f0})}} \\ &\quad\times C^{L_i}_{s_iK_i}C^{L_f}_{s_fK_f}[\cos(\gamma)\langle 20L_iK_i|L_fK_f\rangle\delta_{K_iK_f} \\ &\quad+\frac{1}{\sqrt{2}}\sin(\gamma)\langle 2-2L_iK_i|L_fK_f\rangle\delta_{K_iK_f+2} \\ &\quad+\frac{1}{\sqrt{2}}\sin(\gamma)\langle 22L_iK_i|L_fK_f\rangle\delta_{K_iK_f-2}]\Big\}^2. \end{aligned} \tag{31}$$

Since the rotational function $\varphi^L_{M,s}(\theta_i)$ with $L=0,\,2,\,3,\,5$ defined in Eq. (5) can be analytically solved from Eq. (4), the related $B(E2)$ ratios can be explicitly expressed as

$$\frac{B(E2;3_{\xi_i1}\rightarrow 2_{\xi_f2})}{B(E2;2_{\xi_i1}\rightarrow 0_{\xi_f1})} = \frac{25I^2_\beta(\xi_i,1,3;\xi_f,2,2)}{14I^2_\beta(\xi_i,1,2;\xi_f,1,0)}, \tag{32}$$

$$\frac{B(E2;3_{\xi_i1}\rightarrow 2_{\xi_f1})}{B(E2;2_{\xi_i2}\rightarrow 0_{\xi_f1})} = \frac{25I^2_\beta(\xi_i,1,3;\xi_f,1,2)}{14I^2_\beta(\xi_i,2,2;\xi_f,1,0)}, \tag{33}$$

$$\frac{B(E2;5_{\xi_i1}\rightarrow 3_{\xi_f1})}{B(E2;2_{\xi_i1}\rightarrow 0_{\xi_f1})} = \frac{21I^2_\beta(\xi_i,1,5;\xi_f,1,3)}{22I^2_\beta(\xi_i,1,2;\xi_f,1,0)}, \tag{34}$$

$$\frac{B(E2;5_{\xi_i2}\rightarrow 3_{\xi_f1})}{B(E2;2_{\xi_i2}\rightarrow 0_{\xi_f1})} = \frac{21I^2_\beta(\xi_i,2,5;\xi_f,1,3)}{22I^2_\beta(\xi_i,2,2;\xi_f,1,0)}, \tag{35}$$

$$\frac{B(E2;2_{\xi_i2}\rightarrow 0_{\xi_f1})}{B(E2;2_{\xi_i1}\rightarrow 0_{\xi_f1})} = \frac{I^2_\beta(\xi_i,2,2;\xi_f,1,0)}{I^2_\beta(\xi_i,1,2;\xi_f,1,0)}\tan^2(\gamma+\Gamma), \tag{36}$$

$$\frac{B(E2;2_{\xi_i2}\rightarrow 2_{\xi_f1})}{B(E2;2_{\xi_i2}\rightarrow 0_{\xi_f1})} = \frac{10I^2_\beta(\xi_i,2,2;\xi_f,1,2)}{7I^2_\beta(\xi_i,2,2;\xi_f,1,0)}\frac{\sin^2(\gamma-2\Gamma)}{\sin^2(\gamma+\Gamma)}. \tag{37}$$

It is clear that the results for the ground band and γ band are given by those with $\xi=1$, while the results for the β band are those with $\xi=2$.

3. Numerical examination

As mentioned above, the present model may provide a dynamical connection between the X(4) and the Z(4) CPSs. To demonstrate the connection, some typical energy ratios and $B(E2)$ ratios calculated from related models are given in Table I. As shown in Table I, the T(4) results in the $\gamma=0^\circ$ and $\gamma=30^\circ$ limits indeed reproduce those of the X(4) and the Z(4) CPSs, respectively. Specifically, the ratios E_{L_1}/E_{2_1} and E_{L_ξ}/E_{2_1} in the present T(4) model decrease monotonously from the X(4) limit ($\gamma=0^\circ$) to the Z(4) limit ($\gamma=30^\circ$), while the approximately constant behavior of $E(8_1)/E(0_\xi)\sim 1.8$ for all γ values indicates that this feature can be regarded as a signal of the T(4) CPS, which may be observed experimentally. In short, the T(4) solutions as a function of γ provide a smooth structural evolution from the X(4) CPS to the Z(4) CPS. Since the two CPSs can be applied to describe the nuclei around the critical points of the U(5)-SU(3) and the U(5)-O(6) shape phase transitions [5, 13], respectively, it is thus expect that the T(4) model may play a role as the CPS for more general spherical-deformed shape phase transition in between the U(5)-SU(3) and U(5)-O(6) ones. Typical quadrupole shapes and the associated shape transitions in the IBM are traditionally described by a consistent-Q Hamiltonian [29, 30], which is written as

$$\hat{H}(\eta,\,\chi) = \varepsilon_0\left[(1-\eta)\hat{n}_d - \frac{\eta}{4N}\hat{Q}^\chi\cdot\hat{Q}^\chi\right], \tag{38}$$

where $\hat{Q}^\chi = (d^\dagger s + s^\dagger\tilde{d})^{(2)} + \chi(d^\dagger\tilde{d})^{(2)}$ is the quadrupole operator, η and χ are the control parameters with $\eta\in[0,1]$ and $\chi\in[-\sqrt{7}/2,0]$, and ε_0 is a scale factor. It can be proved

TABLE I: Typical energy ratios and $B(E2)$ ratios for the ground band and the $\xi = 2$ band calculated in the T(4) model with various γ values and compared with the corresponding quantities in the X(4) [13] and the Z(4) [5] as well as those calculated in the U(5), the O(6) and the SU(3) limit of the IBM for $N = 10$. The results with L_ξ correspond to those with $L = 2\tau$ in the first excited families in the U(5) and the O(6) limit, such as the $\sigma = N-2$ family in the O(6)limit, where σ and τ represent the quantum numbers of the O(6) and the O(5), respectively.

	X(4)	T(4)							Z(4)	U(5)	O(6)	SU(3)
		$\gamma=0^\circ$	$\gamma=5^\circ$	$\gamma=10^\circ$	$\gamma=15^\circ$	$\gamma=20^\circ$	$\gamma=25^\circ$	$\gamma=30^\circ$				
E_{4_1}/E_{2_1}	2.71	2.71	2.71	2.69	2.65	2.54	2.34	2.23	2.23	2.00	2.50	3.33
E_{6_1}/E_{2_1}	4.90	4.90	4.89	4.85	4.68	4.31	3.88	3.67	3.67	3.00	4.50	7.00
E_{8_1}/E_{2_1}	7.50	7.50	7.49	7.39	7.00	6.30	5.62	5.32	5.32	4.00	7.00	12.00
E_{8_1}/E_{0_ξ}	1.80	1.80	1.82	1.87	1.88	1.85	1.82	1.80	1.80	2.00	0.64	0.47
E_{0_ξ}/E_{2_1}	4.16	4.16	4.11	3.95	3.71	3.40	3.10	2.95	2.95	2.00	11.00	25.33
E_{2_ξ}/E_{2_1}	6.04	6.04	5.98	5.82	5.57	5.26	4.95	4.80	4.80	3.00	12.00	26.33
E_{4_ξ}/E_{2_1}	9.01	9.01	8.94	8.75	8.42	7.90	7.25	6.89	6.89	4.00	13.50	28.67
$\frac{B(E2;\,4_1\to2_1)}{B(E2;\,2_1\to0_1)}$	1.70	1.70	1.71	1.71	1.75	1.78	1.74	1.71	1.71	1.80	1.38	1.40
$\frac{B(E2;\,6_1\to4_1)}{B(E2;\,2_1\to0_1)}$	2.16	2.16	2.17	2.20	2.30	2.43	2.29	2.41	2.41	2.40	1.52	1.48
$\frac{B(E2;\,8_1\to6_1)}{B(E2;\,2_1\to0_1)}$	2.51	2.51	2.52	2.58	2.76	2.99	3.02	2.91	2.91	2.80	1.55	1.45
$\frac{B(E2;\,0_\xi\to2_1)}{B(E2;\,2_1\to0_1)}$	0.95	0.95	0.96	0.98	1.01	1.06	1.12	1.15	1.15	1.80	0.00	0.00
$\frac{B(E2;\,2_\xi\to0_\xi)}{B(E2;\,2_1\to0_1)}$	0.81	0.81	0.81	0.81	0.80	0.79	0.78	0.77	0.77	1.12	0.68	0.74

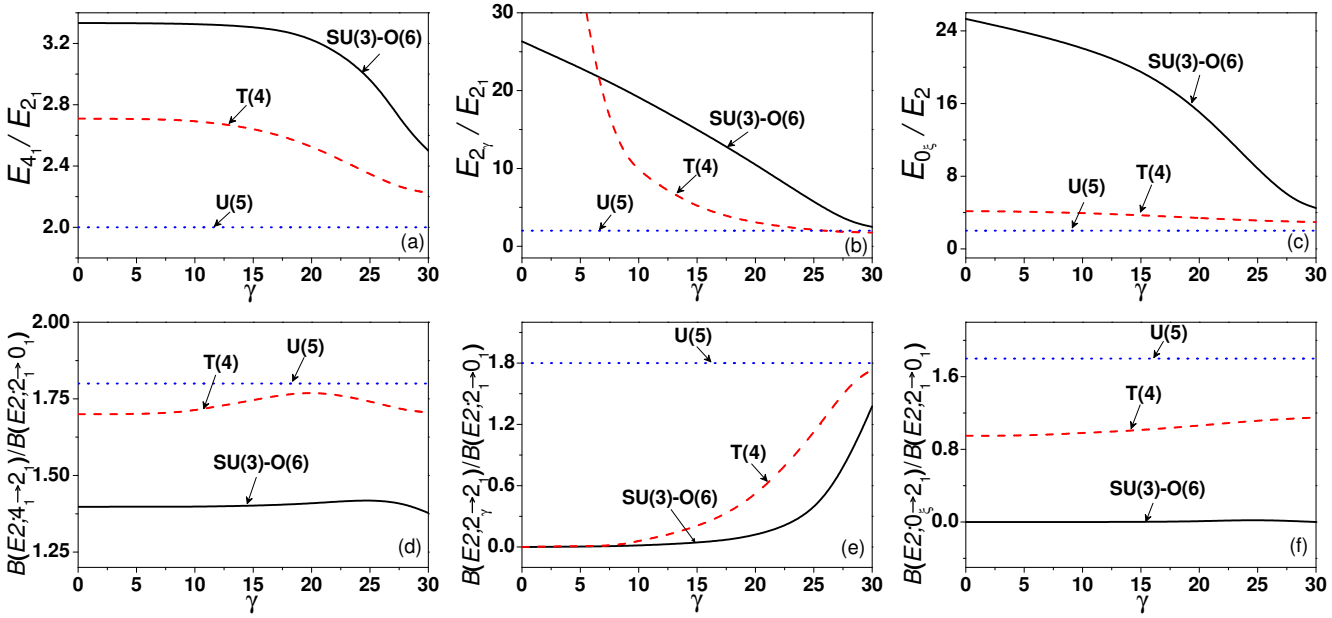

FIG. 1: (Color online) Selected energy ratios and $B(E2)$ ratios of the T(4) model and IBM for $N = 10$ as functions of γ (in degree) with the assumption $\gamma(\chi) = \frac{\pi}{3\sqrt{7}}\chi + \frac{\pi}{6}$ for the IBM.

that the Hamiltonian is in the U(5) symmetry limit corresponding to spherical vibration when $\eta = 0$, the O(6) symmetry limit corresponding to γ-unstable rotation when $\eta = 1$ and $\chi = 0$, and the SU(3) symmetry limit corresponding to axially-symmetric rotation when $\eta = 1$ and $\chi = -\sqrt{7}/2$. This Hamiltonian can be used to describe the phase transitions from the spherical shape (corresponding to the U(5) limit) to the deformed shape (corresponding to either the SU(3) limit or the O(6) limit or their mixing). As shown in Table I, the energy ratios and the $B(E2)$ ratios in the T(4) model almost all locate in between those around the U(5) point and those in the SU(3) limit or the O(6) limit, which in turn hints that T(4) may be suitable to describe more general spherical-deformed shape phase transitions.

To realize the calculation of γ dependence explicitly in the IBM, for instance the SU(3)-O(6) crossover [20, 31], we propose a linear relation between γ and χ with $\gamma(\chi) = \frac{\pi}{3\sqrt{7}}\chi + \frac{\pi}{6}$,

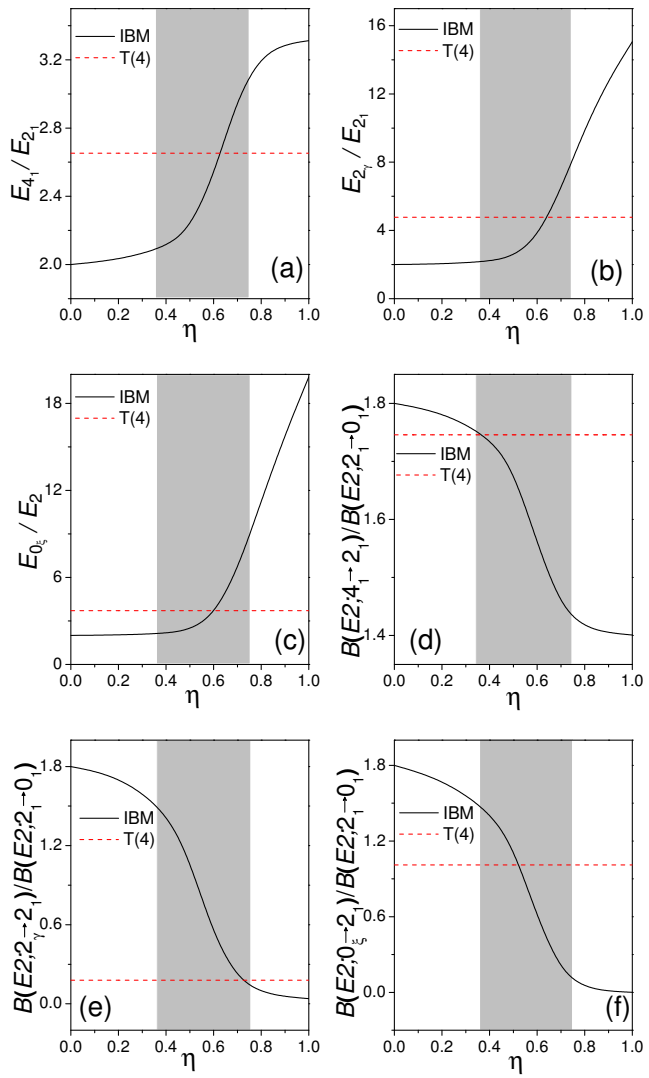

FIG. 2: (Color online) Transitional behaviors of typical energy rations and $B(E2)$ ratios as functions of η in the IBM for $N=10$ solved from the Hamiltonian (38) with $\chi=-\sqrt{7}/4$ and the corresponding results obtained from the T(4) model at $\gamma=\pi/12$ based on the assumption $\gamma(\chi)=\frac{\pi}{3\sqrt{7}}\chi+\frac{\pi}{6}$.

which agrees with the point that the SU(3) limit ($\chi=-\sqrt{7}/2$) describes the prolate-rotor corresponding to $\gamma=0$ and the O(6) limit ($\chi=0$) corresponds to the algebraical triaxial rotor with $\gamma_{\rm av}=\pi/6$ since, in the mean-field level, it has γ-flat potential oscillating uniformly over γ from 0 and $\pi/3$ [21, 22]. This simple assumption also agrees with the point that the SU(3) limit ($\chi=\sqrt{7}/2$) corresponds to the oblate-rotor with $\gamma=\pi/3$. We can thus carry out the calculation and make a comparison between our T(4) model and the IBM within $\gamma\in[0,\ 30^\circ]$. Some typical quantities calculated in the two models as functions of γ are shown in Fig. 1.

It can be seen from Fig. 1 that the results in the U(5) limit keep as the constants as expected and those in the T(4) model and the IBM along the SU(3)-O(6) transition line may either dramatically or slightly change as functions of γ. More importantly, the energy ratios and $B(E2)$ ratios in the T(4) model almost all locate between the counterparts of the U(5) limit and the SU(3)-O(6) line for any value of $\gamma\in[0^\circ,\ 30^\circ]$, which further confirms that the T(4) model with a given γ value, similar to Z(4) and X(4), is reasonable to be taken as the CPS of a more general spherical-deformed shape transition (transition from the U(5) point to a point on the SU(3)-O(6) line). One can further observe that the energy ratio E_{2_γ}/E_{2_1} may be taken as an indicator of the γ value for the T(4) model because this quantity is very sensitive to γ. Once the γ value is fixed by fitting the experimental energy ratio E_{2_γ}/E_{2_1}, the whole spectral structure is determined by the model up to an overall scale factor. However, the γ-rigid nature of the T(4) model makes the values of E_{2_γ}/E_{2_1} with $\gamma<6^\circ$ are too high to accommodate a realistic situation as seen from Fig. 1(b). It means that the T(4) model in a very small γ-deformation or the axially-symmetric case ($\gamma=0^\circ$) corresponding to X(4) cannot be used to describe γ-vibration in experiments. In contrast, all the other quantities in the T(4) model change little with $\gamma\in[0^\circ,\ 6^\circ]$, which in turn indicates that the cases within $\gamma\in[6^\circ,\ 30^\circ]$ may cover all the realistic situations in the T(4) model including the reasonable γ-vibration.

To further check the CPS role played by the T(4) model, we take the spherical-deformed transitional line in the IBM characterized with $\chi=-\sqrt{7}/4$ and $\eta\in[0,\ 1]$ as an example, of which the parameter trajectory is located in between the one of U(5)-SU(3) transition corresponding to $\chi=-\sqrt{7}/2$ and that of U(5)-O(6) transition corresponding to $\chi=0$. Specifically, the evolutional behaviors of several typical quantities as functions of η calculated from IBM for $N=10$ are shown in Fig. 2 to compare with the corresponding results in the T(4) model at $\gamma=\pi/12$ (15°) based on the relation $\gamma(\chi)=\frac{\pi}{3\sqrt{7}}\chi+\frac{\pi}{6}$ defined above. As seen from Fig. 2, all quantities in the IBM as functions of η show rapid changes within the range of $\eta\simeq 0.35\sim 0.75$ denoted by the dark area, which could be regarded as the precursors of the spherical-deformed shape phase transition in a finite-N case [30]. More importantly, the T(4) results (see the crossing point between T(4) and IBM) are almost all located in the rapidly changing region of the spherical-deformed transition in the IBM, which further justifies that the T(4) model should be qualified to be taken the CPS for a more general spherical-deformed shape phase transitions in nuclei.

Similar to the original T(5) model [12], the T(4) model may also behave as the β-soft triaxial rotor. However, the γ variable in the T(4) model is a deformation parameter indicating the axial-asymmetry of the system, which makes the model exactly solvable, while γ is a dynamical variable in the T(5) model, of which only approximate solutions can be obtained [12]. It is worth mentioning that it may become possible to obtain accurate numerical solutions of the X(5) or the T(5)-like models [32] due to the development of numerical diagonalization methods for the Bohr Hamiltonian [32–37]. In addition, the Z(4) limit or the large γ cases in the T(4) CPS model may be applied to describe the E(5)-like nuclei since the predictions of the energy ratios and $B(E2)$ ratios of the Z(4) CPS are in close agreement with those of the E(5)

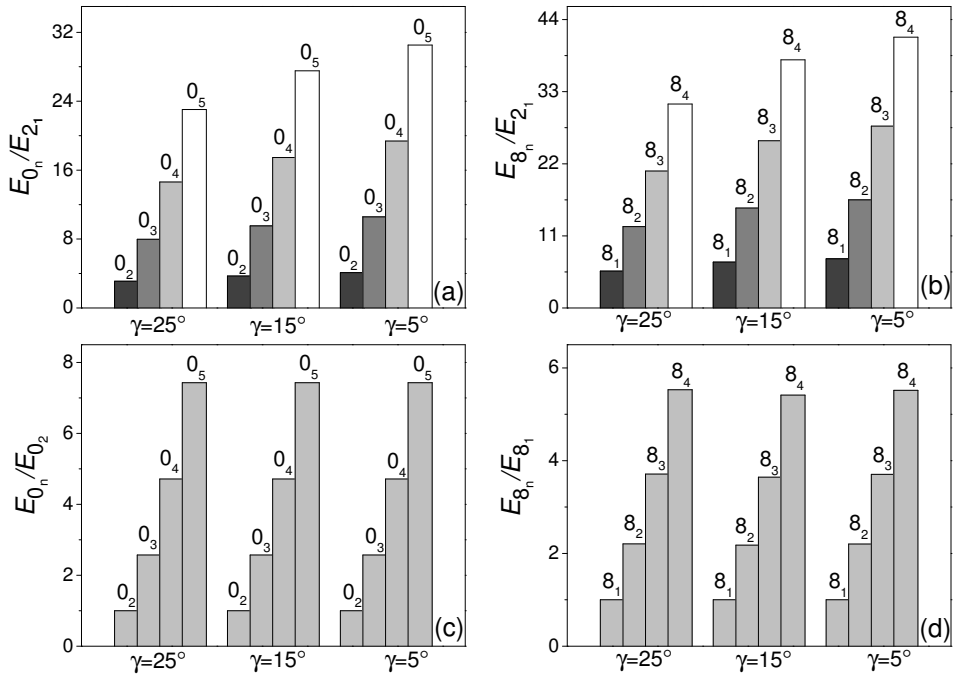

FIG. 3: (Color online) The energy ratios E_{0_n}/E_{2_1}, E_{8_n}/E_{2_1}, E_{0_n}/E_{0_2} and E_{8_n}/E_{8_1} calculated in the T(4) model for $\gamma = 5^\circ,\ 15^\circ,\ 25^\circ$, where E_{0_n} with $n = 1,\ 2,\ 3,\ 4,\ 5$ are the bandhead energies, and E_{8_n} with $n = 1,\ 2,\ 3,\ 4$ represent the energy values of the states with $L_{\xi,\,s} = 8_{n,\,1}$.

CPS [5]. While the cases with large γ values in the T(5) CPS are suitable to describe the O(6)-like nuclei, such as the Pt isotopes with $A = 192$-196 [4, 12].

Another point worth to be mentioned is that the constant behavior $E_{8_1}/E_{0_\beta} \sim 1.8$ in the T(4) model is due to the fact that $v_{\mathrm{T}(4)}$ in Eq. (24) for both $L = 0$ and $L = 8$ changes little with variation of γ value. As a further analysis, the related energy ratios calculated with several typical γ values are shown in Fig. 3. One can see from Fig. 3(a) that the bandhead energies E_{0_n} with $n = 2,\ 3,\ 4,\ 5$ all monotonically increase with the decreasing of γ if they are normalized to E_{2_1}. However, if these bandhead energies are normalized to E_{0_2} as shown in Fig. 3(c), they all keep to be respective constant independent of γ, which approximately coincides with the rule [38, 39] with

$$E_{0_n} = E_0(n-1)(n+3/2), \tag{39}$$

where E_0 is an overall scale factor independent of γ. The rule in Eq. (39) is actually the reflection of E(4) dynamical symmetry as analyzed in Ref. [38, 39], which in turn indicates that the T(4) solutions may serve as a partial dynamical symmetry of type I (some of the states follow exactly the dynamical symmetry) [40]. The similar situation also occurs for E_{8_n} with $n = 1,\ 2,\ 3,\ 4$ as shown in Fig. 3(b) and Fig. 3(d), where E_{8_n} decrease as functions of γ when normalized to E_{2_1}, but approximately constants if been normalized to E_{8_1}.

4. Comparison to experiment

As shown in previous sections, the T(4) model may provide a dynamical connection between the X(4) CPS [13] and the Z(4) CPS [5] via γ deformation from $\gamma = 0^\circ$ to $\gamma = 30^\circ$. Since the Z(4) and X(4) CPS, which correspond to the maximally triaxial limit ($\gamma = 30^\circ$), the axially-symmetric limit ($\gamma = 0^\circ$), respectively, of our T(4) model, have been experimentally confirmed [5, 13], it would be significant to test the validity of the model with an intermediate γ-deformation.

In the following, ^{158}Er [41] is chosen as a candidate of the T(4) model with an intermediate γ-deformation. Although ^{158}Er and other rare-earth nuclei with the neuron number $N_n = 90$ are allocated with the fixed β-values in [43] according to a given formula (Eq. (2) in Ref. [43]), these nuclei could be alternatively connected with the β-potential of a flat bottom as they are usually considered to be close to the critical points of spherical to deformed shape phase transitions [15, 44]. Moreover, the possible β-soft and triaxial deformation existing in ^{158}Er is also consistent with the recent analysis of the Er isotopes given in [45]. In the concrete calculations, the γ value in the T(4) model is determined by a global fit to experimental values of 16 low-lying levels in ^{158}Er based on the root mean square defined as $R = \sqrt{\frac{1}{n}\sum_{i=1}^{n}(A^i_{\mathrm{theo.}} - A^i_{\mathrm{exp.}})^2}$. It is found that T(4) with $\gamma = 14.7^\circ$ may provide a globally well fit to the experimental data, with $R = 0.15$MeV. Notably, once the γ value is given, the entire spectral structure of the T(4) model would be fixed up to a scale factor. As a comparison, calculations in the IBM are also carried out with the parameters N, η and χ in Eq. (38) taken from Ref. [42]. With the same experimental data, it is given by $R = 0.21$MeV for the IBM calculations under the parameters used in [42].

To have a close look at the related results, the low-lying levels of the ground band, β band and γ band in ^{158}Er and

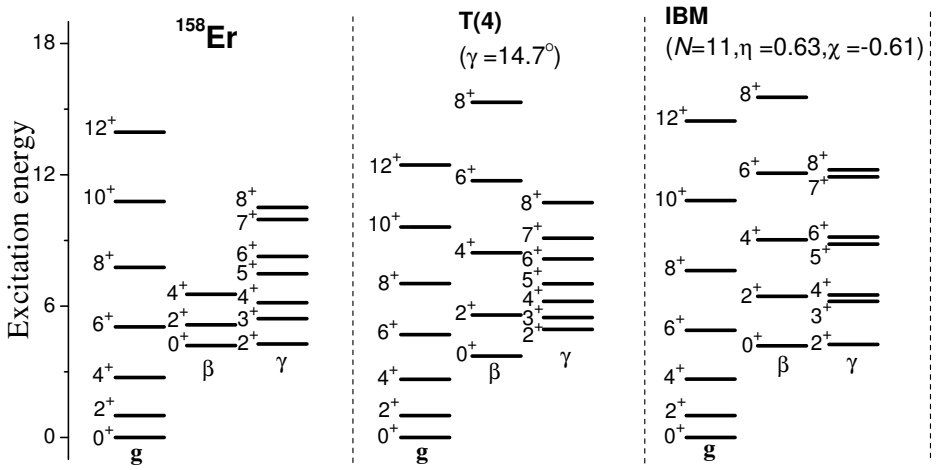

FIG. 4: (Color online) The low-lying level patten of ^{158}Er [41] and those solved from the T(4) model and the IBM, where all level energies have been normalized to $E(2_1)$ in each case. In calculations, the γ value in the T(4) model is set as $\gamma = 14.7^\circ$, and the parameters in the IBM Hamiltonian (38) are taken as $N = 11$, $\eta = 0.63$, and $\chi = -0.61$, which are the same as those adopted in Ref. [42].

those obtained from the T(4) model and IBM are shown in Fig. 4. Some typical energy ratios and $B(E2)$ ratios in theories together with corresponding experimental data are listed in Table II to make a further comparison. As seen from Fig. 4, the spectral pattern in the T(4) model with $\gamma = 14.7^\circ$ shows similar to the one obtained from the IBM, and both models present generally well reproduction of the experimental data for both band head positions and the band structures. In addition, it can be found that the spacing of level energies in the β band is over predicted by both models, and this point cannot be improved by adjusting the γ value in the T(4) model. The similar situation is also encountered in the X(5) CPS [2] when comparing the experimental data as the larger β-band spacings in these models are mainly due to the steep finite "wall" in the potential as a function of β [9]. This drawback in the T(4) model can be removed to some extent either by involving a sloped wall in the infinite potential as done in [9] or by replacing the infinite square well with a potential with a finite wall at large β like the Kratzer potential discussed in [46]. The differences between the IBM and T(4) in the present case are mainly embodied in the γ bands. In the IBM, the levels in the γ band show strong odd-even staggering with couples arranged as (2^+_γ), $(3^+_\gamma, 4^+_\gamma)$, $(5^+_\gamma, 6^+_\gamma)$, ... In contrast, only slightly odd-even staggering with the opposite sign is observed in the T(4) model with the levels in the γ band coupled as $(2^+_\gamma, 3^+_\gamma)$, $(4^+_\gamma, 5^+_\gamma)$, $(6^+_\gamma, 7^+_\gamma)$, ... In experiments, the odd-even staggering effect in the γ band is relatively weak like in the T(4) model but the sign of staggering is opposite to the one in the T(4) model. Although the IBM description presents stronger staggering than in the experiment, it has the right sign. Band-mixing mechanism is often used to explain the odd-even staggering in the γ band in different models. For example, both the presence and sign of the odd-even staggering effects in some heavy deformed nuclei can be well explained by the ground-γ bands mixing in the framework of the vector boson model with the SU(3) dynamical symmetry [47]. In the SU(3) limit of the IBM [20], the odd-even staggering in the γ band can be alternatively explained as the β-γ bands mixing, through considering high-order interactions. One of the common points in the above two methods is to find a way to make all the states in the two mixing bands fall into the SU(3) irreducible representation $(\lambda,\ \mu = 2)$ with $\lambda \gg \mu$, which in turn guarantees that only the $K = 0$ and $K = 2$ bands are allowed to exist in the same SU(3) representation. Here, the staggering feature in the T(4) model could be associated with the γ-rigid nature of the model and may be explained as the the ground-γ bands mixing as in the Davydov rotor [26] based on the analysis in [21] since both the ground band and γ band correspond to $\xi = 1$ while the β band corresponds to $\xi = 2$ in the T(4) model as discussed in Section 2. On the other hand, the odd-even staggering effects in the present IBM calculations are mainly due to the O(6) components involving in the Hamiltonian [21], while the O(6) dynamics up to two-body interactions can be associated with a γ-independent potential in the mean-field level [20].

It can be further found in Table II that the typical energy ratios and $B(E2)$ ratios in experiments are generally well reproduced in the IBM and the T(4) model. Particularly, the ratio E_{8_g}/E_{0_β} maintains approximately a constant 1.8 in both experimental and theoretical cases. One can also find that the intraband transitions in the T(4) model are qualitatively stronger than those in the IBM but the global similarity between the two models are sustained. Anyway, it manifests that the T(4) model indeed provides a reasonable description of ^{158}Er, which, in turn, indicates that possible triaxial deformation may be involved to some extent in this critical point nucleus.

TABLE II: Some typical energy ratios and $B(E2)$ ratios in ^{158}Er [41] and the ones calculated from the T(4) with $\gamma = 14.7^\circ$ model and the IBM with $N = 11,\ \eta = 0.63,\ \chi - 0.61$, where "—-" denotes the corresponding quantity is not determined experimentally.

Energy ratios	^{158}Er	T(4)	IBM	B(E2) ratios	^{158}Er	T(4)	IBM
E_{4_g}/E_{2_g}	2.74	2.66	2.66	$\frac{B(E2;\,4_g\to 2_g)}{B(E2;\,2_g\to 0_g)}$	1.49	1.74	1.52
E_{6_g}/E_{2_g}	5.05	4.70	4.89	$\frac{B(E2;\,6_g\to 4_g)}{B(E2;\,2_g\to 0_g)}$	2.02	2.29	1.73
E_{8_g}/E_{0_β}	1.85	1.89	1.82	$\frac{B(E2;\,8_g\to 0_g)}{B(E2;\,2_g\to 0_g)}$	2.61	2.75	1.82
E_{0_β}/E_{2_g}	4.20	3.72	4.18	$\frac{B(E2;\,0_\beta\to 2_g)}{B(E2;\,2_g\to 0_g)}$	——	1.01	0.41
E_{2_β}/E_{2_g}	5.15	5.59	6.44	$\frac{B(E2;\,2_\beta\to 0_\beta)}{B(E2;\,2_g\to 0_g)}$	——	0.80	0.55
E_{2_γ}/E_{2_g}	4.27	4.94	4.25	$\frac{B(E2;\,2_\gamma\to 2_g)}{B(E2;\,2_g\to 0_g)}$	——	0.17	0.40
E_{3_γ}/E_{2_g}	5.43	5.48	6.22	$\frac{B(E2;\,3_\gamma\to 2_\gamma)}{B(E2;\,2_g\to 0_g)}$	——	2.73	0.92

5. Summary

In summary, the γ-rigid solutions of the Bohr Hamiltonian with an infinite square well for the β-potential, called T(4), have been worked out for $\gamma \in [0^\circ,\ 30^\circ]$. It was shown that the original X(4) [13] and Z(4) CPSs [5] can be naturally realized within the T(4) model in the $\gamma = 0^\circ$ and $\gamma = 30^\circ$ limit, respectively. It thus offers a new and flexible CPS description of the critical point symmetry nuclei in the spherical to γ-rigidly deformed or to γ-unstable shape phase transition. Comparison to the IBM calculations further supports that the T(4) dynamics with $\gamma \in [0^\circ,\ 30^\circ]$ is appropriate to describe the transitions between the spherical with U(5) and the deformed structures like SU(3), O(6) or their mixing. Some key spectral features of the T(4) model are also identified. In experiments, ^{158}Er provides the possible candidate of the T(4) CPS with an intermediate γ-deformation through comparing the experimental data with those theoretical calculations, which confirms that the T(4) CPS can indeed provide a simple but effective way to describe the nuclei close to the critical point of the general spherical-deformed transition.

Our previous work shows that the algebraic model based on the Euclidean dynamical symmetry [48], called F(5), can build a link between the E(5) and the X(5) CPS dynamics, which, thus, provides a unified description of the structural evolution in the spherical to deformed shape phase transitions. The present T(4) model provides an alternative way to describe the similar physical situation. A comparison between the two different schemes should be interesting. In addition, the T(4) solution may provide a convenient starting point to establish an alternative CPS description for triaxial odd-A nuclei in the transitional region in contrast to those shown in Ref. [49–55], which have been mostly applied to the axially-deformed or the γ-unstable situations. While the T(4) model enables to describe the critical point of the shape phase transition in between the two. Related works are in progress.

Acknowledgments

Support from the Natural Science Foundation of China (11375005, 11675071, 11375080, 11435001 and 11475091), U. S. National Science Foundation (OCI-0904874), Southeastern Universities Research Association, and the LSU–LNNU joint research program (9961) is acknowledged. YXL thanks also the support from the National Key Basic Research Program of China under Contracts No. G2013CB834400.

[1] F. Iachello, Phys. Rev. Lett. **85**, 3580 (2000).
[2] F. Iachello, Phys. Rev. Lett. **87**, 052502 (2001).
[3] F. Iachello, Phys. Rev. Lett. **91**, 132502 (2003).
[4] D. Bonatsos, D. Lenis, D. Petrellis, and P. A. Terziev, Phys. Lett. B **588**, 172 (2004).
[5] D. Bonatsos, D. Lenis, D. Petrellis, P. A. Terziev, and I. Yigitoglu, Phys. Lett. B **621** 102 (2005).
[6] D. Bonatsos, D. Lenis, D. Petrellis, P. A. Terziev, and I. Yigitoglu, Phys. Lett. B **632**, 238 (2006).
[7] D. Bonatsos, D. Lenis, N. Minkov, D. Petrellis, P. P. Raychev, and P. A. Terziev, Phys. Rev. C **70**, 024305 (2004).
[8] M. A. Caprio, Phys. Rev. C **65**, 031304(R) (2002).
[9] M. A. Caprio, Phys. Rev. C **69**, 044307 (2004).
[10] L. Fortunato, Phys. Rev. C **70**, 011302(R) (2004).
[11] N. Pietralla and O. M. Gorbachenko, Phys. Rev. C **70**, 011304(R) (2004).
[12] Y. Zhang, F. Pan, Y. A. Luo, and J. P. Draayer, Phys. Lett. B **751** 423 (2015).
[13] R. Budaca and A. I. Budaca, Phys. Lett. B **759** 349 (2016).
[14] R. F. Casten and E. A. McCutchan, J. Phys. G **34**, R285 (2007).
[15] P. Cejnar, J. Jolie, and R. F. Casten, Rev. Mod. Phys. **82**, 2155 (2010).
[16] L. Fortunato, Eur. Phys. J. A **26**, s01, 1 (2005).
[17] A. Bohr, Mat.-Fys. Medd. Danske Vid. Selsk. **26**, No. 14 (1952)
[18] P. Buganu and R. Budaca, Phys. Rev. C **91** 014306 (2015).
[19] P. Buganu and R. Budaca, J. Phys. G, Nucl. Part. Phys. **42** 105016 (2015).
[20] F. Iachello, and A. Arima, The Interacting Boson Model, Cambridge University, Cambridge, England, 1987.
[21] N. V. Zamfir, R. F. Casten, Phys. Lett. B **260** 265 (1991).
[22] R. F. Casten, Nuclear Structure from a Simple Perspective, Oxford Univ. Press, Oxford, 1990.
[23] A. S. Davydov and A. A. Chaban, Nucl. Phys. A **20** 499 (1960).
[24] W. Greiner and J. A. Maruhn, Nuclear Models, Springer-Verlag, Berlin, 1996.
[25] Q. Y. Li, X. X. Wang, Y. Zuo, Y. Zhang, and F. Pan, Chin. Phys. C **40** 014101 (2016).
[26] A. S. Davydov and G. F. Fillipov, Nucl. Phys. **8**, 237 (1958).
[27] J. L. Wood, A. M. Oros-Peusquens, R. Zaballa, J. M. Allmond, and W. D. Kulp, Phys. Rev. C **70**, 024308 (2004); J. M. Allmond, Ph.D. dissertation, Georia Institute of Technology (2007), http://hdl.handle.net/1853/14604.
[28] A. R. Edmonds, Angular Momentum in Quantum Mechanics, Princeton Univ. Press, Princeton, 1957.
[29] D. D. Warner and R. F. Casten, Phys. Rev. C **28**, 1798 (1983).
[30] F. Iachello and N. V. Zamfir, Phys. Rev. Lett. **92**, 212501

(2004).
[31] J. Jolie, R. F. Casten, P. von Brentano, and V. Werner, Phys. Rev. Lett. **87**, 162501 (2001).
[32] M. A. Caprio, Phys. Rev. C **72**, 054323 (2005).
[33] D. J. Rowe, Nucl. Phys. A **735**, 372 (2004).
[34] D. J. Rowe, P. S. Turner, and J. Repka, J. Math. Phys. **45**, 2761 (2004).
[35] D. J. Rowe and P. S. Turner, Nucl. Phys. A **753**, 94 (2005).
[36] D. J. Rowe, T. A. Welsh, and M. A. Caprio, Phys. Rev. C **79**, 054304 (2009).
[37] G. Thiamova, D. J. Rowe, and M. A. Caprio, Nucl. Phys. A **895**, 20 (2012).
[38] D. Bonatsos, E. A. McCutchan, and R. F. Casten, Phys. Rev. Lett. **101**, 022501 (2008).
[39] D. Bonatsos, E. A. McCutchan, R. F. Casten, R. J. Casperson, V. Werner, E. Williams, Phys. Rev. C **80**, 034311 (2009).
[40] A. Leviatan, Phys. Rev. Lett. **98**, 242502 (2007).
[41] R. G. Helmer, Nucl. Data Sheets **101**, 325 (2004).
[42] E. A. McCutchan, N. V. Zamfir, and R. F. Casten, Phys. Rev. C **69**, 064306(2004).
[43] S. Raman, C. W. Nestor, JR., and P. Tikkanen, Atomic Data and Nuclear Data Tables **78**, 1(2001).
[44] R. F. Casten, Nat. Phys. **2**, 811(2006).
[45] F. Q. Chen and J. L. Egido, Phys. Rev. C **95**, 024307 (2017).
[46] D. Bonatsos, P. E. Georgoudis, N. Minkov, D. Petrellis, and C. Quesne, Phys. Rev. C **88**, 034316 (2013).
[47] N. Minkov, S. B. Drenska, P. P. Raychev, R. P. Roussev, and D. Bonatsos, Phys. Rev. C **61**, 064301 (2000).
[48] Y. Zhang, Y. X. Liu, F. Pan, Y. Sun, and J. P. Draayer, Phys. Lett. B **732**, 55 (2014).
[49] F. Iachello, Phys. Rev. Lett. **95**, 052503 (2005).
[50] C. E. Alonso, J. M. Arias, and A. Vitturi, Phys. Rev. Lett. **98**, 052501 (2007).
[51] C. E. Alonso, J. M. Arias, and A. Vitturi, Phys. Rev. C **75**, 064316 (2007).
[52] Y. Zhang, F. Pan, Y. X. Liu, Z. F. Hou, and J. P. Draayer, Phys. Rev. C **82**, 034327 (2010).
[53] Y. Zhang, F. Pan, Y. X. Liu, Y. A. Luo, and J. P. Draayer, Phys. Rev. C **84**, 034306 (2011).
[54] Y. Zhang, F. Pan, Y. X. Liu, and J. P. Draayer, Phys. Rev. C **84**, 054319 (2011).
[55] Y. Zhang, F. Pan, Y. A. Luo, Y. X. Liu, and J. P. Draayer, Phys. Rev. C **86**, 044312 (2012).